Optimally Efficient Thrust Generation in Heaving, Pitching, and Chordwise-Extending Plates

Logan Edwards

Mentored by Dr. Silas Alben and Pranav Jois

Abstract

Motivated by biological propulsion, we investigate the efficiency of periodic motions combining heaving, pitching, and chordwise-morphing. We utilize a vortex sheet method to model the effects of these motions on a thin, flat plate immersed in inviscid fluid. We identify several sets of motion which produce thrust with good efficiency. We also investigate the dynamics associated with particular parameter sets obtained with a gradient-based optimization, obtaining new insight into potential mechanisms for efficient thrust generation in chordwise lengthening and retracting bodies.

Contents

1 Introduction **2**

2 Methods **2**
2.1 Body Parameterization 2
2.2 Mathematical Model 3
2.3 Desingularized Model 5
2.4 Numerical Method 6
2.4.1 Bound Sheet 6
2.4.2 Free Sheet 7
2.4.3 Performance Metrics 8
2.5 Optimization Method 8

3 Preliminary Results **9**
3.1 Dynamics of Lengthening-Based Maneuvers 10

4 Discussion and Future Work **11**

5 Conclusion **12**

6 Acknowledgments **12**

References **12**

A Pressure Jump Equation **13**

1 Introduction

The aerodynamic performance of airfoils is of particular importance in many areas of engineering. Inspired by biological mechanisms observed in birds, bats, and marine organisms, the experimental work of Van Buren, Floryan, and Smits [15] identifies propulsively efficient combinations of pitching and heaving in thin airfoils, while the work of Steele et al. [14] has shown that retractive motions on streamlined bodies, with a gradual shrinking in planar profile, can alter the wake and produce additional thrust. Recent computational works have found that chordwise extension and retraction can improve propulsive efficiency in thin plates when superimposed with plunging [8] or combined pitching and heaving [3].

Few studies have been performed varying pitching, heaving, and chordwise morphing in combination, likely due in part to the large number of experiments necessary to identify efficient parameter sets. If computational methods are utilized, a gradient-based optimization approach can substantially reduce the number of necessary numerical experiments. However, standard methods in computational fluid dynamics (CFD), including lattice Boltzmann methods (LBM) as utilized in Cong et al. [3] or Reynolds-averaged Navier Stokes (RANS) solvers utilized in Liu et al. [8], are often too computationally expensive to pair with an optimization algorithm.

In the present work, we investigate combined pitching, heaving, and chordwise lengthening and retraction in two-dimensional flat plates using a vortex sheet method. Vortex sheet methods have been used to model flapping plates, where good agreement is shown in the wake structures and circulations when compared with direct numerical simulation (DNS) at moderate Reynolds numbers [13]. Other works have found good agreement in forces when compared with experiments [6]. Importantly, vortex sheet methods are relatively computationally inexpensive for short and moderate time simulations, making them well-suited for studying periodic motions and enabling investigation of a larger parameter space. We leverage this fact to vary the magnitudes and phase differences of prescribed sinusoidal pitching, heaving, and chordwise extension, utilizing the quasi-Newton method L-BFGS-B to obtain approximate parameters which optimize the Froude efficiency at several frequency values.

2 Methods

2.1 Body Parameterization

The purpose of this section is to describe the types of motion which are to be studied in the current work. We consider a two-dimensional flat plate, which has historically been the basis for modeling thin, symmetric airfoils [2]. We parameterize the body in terms of its heaving, pitching, and extension-retraction motions. We assume these motions are sinusoidal in time, given respectively by

$$h(t) = h_0 \sin(2\pi f t) \tag{1}$$

$$\theta(t) = \theta_0 \sin(2\pi f t + \phi_\theta) \tag{2}$$

$$L(t) = 1 + \frac{L_0}{2} \sin(2\pi f_L t + \phi_L) \tag{3}$$

where h_0 and θ_0 are the amplitudes of heaving and pitching respectively, ϕ_θ and ϕ_L are the phase differences between pitching and lengthening relative to heaving, and $L_0 \in [0, 2)$ is the difference between the maximum and minimum chord length. Pitching and heaving both occur with the same frequency, f, and we consider lengthening at frequencies $f_L = f$ and $f_L = 2f$. We fix material coordinates $\alpha \in [-1, 1]$, and we define the arclength $s(\alpha, t)$ in terms of $L(t)$,

$$s(\alpha, t) = L(t)(\alpha - \alpha_0) \tag{4}$$

where $\alpha_0 \in [-1, 1]$ is the pivot location. We assume that the pivot location travels, from left to right, with a horizontal speed U. With this, the motion of a point $z(s(\alpha, t), t)$ on the body is fully prescribed:

$$z(s(\alpha, t), t) = ih(t) + s(\alpha, t)e^{i\theta(t)} + Ut \tag{5}$$

Finally, we define the unit normal $\hat{n}(t)$ and unit tangent $\hat{s}(t)$ to the plate in complex notation,

$$\hat{n}(t) = ie^{i\theta(t)} \tag{6}$$

$$\hat{s}(t) = e^{i\theta(t)} \tag{7}$$

where $\hat{s}(t)$ points towards the leading edge of the plate, and $\hat{n}(t)$ points above the plate. We characterize the motion by its non-dimensional reduced frequency, f^*, defined by

$$f^* = \frac{fc}{U} \tag{8}$$

where c is the mean chord length and U is the horizontal speed of the pivot location.

2.2 Mathematical Model

The purpose of this section is to introduce the equations which govern the evolution of the fluid-body system in time. We assume that the plate is started impulsively from rest at time $t = 0$ in two-dimensional, inviscid, quiescent background fluid, and that the body follows a prescribed motion of the form described in Section 2.1.

In the inviscid limit, the thickness of the boundary layer shrinks to 0, resulting in a tangential velocity discontinuity, equivalent to superimposing a vortex sheet over the boundary of the body [4]. For an infinitely thin plate, the vortex sheets above and below the body coincide as a single vortex sheet, with sheet strength, $\gamma(\alpha, t)$, defined as the jump in tangential velocity across the sheet:

$$\gamma(\alpha, t) = u^+(\alpha, t) - u^-(\alpha, t) \tag{9}$$

Here, $u^{\pm}(\alpha, t)$ are the magnitudes of tangential fluid velocity just above and just below the sheet respectively [12]. The vortex sheet coinciding with the body is known as the bound sheet, and we denote the set of points comprising it $C^b \subseteq \mathbb{C}$.

The motion of the body causes some vorticity to be shed into the surrounding fluid. In the absence of viscosity, the resulting wake behind the plate is a vortex sheet, which advects vorticity away from the body. For small-amplitude motions, fluid above and below the body remains attached until the trailing edge, at which point it joins and separates from the body as a single vortex sheet, referred to as the free vortex sheet [4]. We refer to the set of points comprising the free vortex sheet as $C^- \subseteq \mathbb{C}$.

At $t = 0$, the body is impulsively started, and vorticity is generated in the bound vortex sheet. The result is the formation of the free sheet, starting as a point at the trailing edge and growing with time. The free and bound vortex sheets can be viewed as a single continuous combined vortex sheet, $C := C^- \cup C^b$. In general, the Birkhoff-Rott equation governs the velocity of a point $z \in C$,

$$\frac{\partial \overline{z}}{\partial t}(s, t) = \frac{1}{2\pi i} \mathrm{PV} \int_C \frac{\gamma(s', t)}{z(s, t) - z(s', t)} \mathrm{d}s' \tag{10}$$

where the PV denotes a principal value integral, and $s \geq s_{\min}$ is a signed arclength along the combined vortex sheet [12]. It is often convenient to parameterize points on the free sheet by their circulation. Consider a point $z(s, t) \in C^-$, where $s \geq s_{\min}$ is a signed arclength parameterizing the free sheet. The circulation, $\Gamma(s, t)$, is defined by the integral

$$\Gamma(s, t) := \int_{s_{\min}}^{s} \gamma(s', t) \mathrm{d}s' \tag{11}$$

where $\gamma(s, t)$ is the vortex sheet strength along the free sheet. Since the free sheet is not yet formed at $t = 0$, it is initially marked by 0 circulation. Therefore, at each time, the evolution of the free vortex sheet is given by

$$\frac{\partial \overline{z}}{\partial t}(\Gamma, t) = \frac{1}{2\pi i} \left(\mathrm{PV} \int_0^{\Gamma^-(t)} \frac{\mathrm{d}\Gamma'}{z(\Gamma, t) - z(\Gamma', t)} + \int_{s(-1,t)}^{s(1,t)} \frac{\gamma(s', t)}{z(\Gamma, t) - z(s', t)} \mathrm{d}s' \right) \tag{12}$$

where $\Gamma^-(t)$ is the total circulation in the free sheet, $s(\pm 1, t)$ are the arclengths corresponding to the leading and trailing edge respectively, and PV again denotes the principal value integral. In terms of material coordinates, the evolution of a point $z(\Gamma, t)$ on the free sheet is given by Mavroyiakoumou and Alben [11],

$$\frac{\partial \overline{z}}{\partial t}(\Gamma, t) = \frac{1}{2\pi i} \left(\int_{-1}^{1} \frac{\gamma(\alpha, t)}{z(\Gamma, t) - z(\alpha, t)} \frac{\partial s}{\partial \alpha}(t) \, \mathrm{d}\alpha + \mathrm{PV} \int_0^{\Gamma^-(t)} \frac{\mathrm{d}\Gamma'}{z(\Gamma, t) - z(\Gamma', t)} \right) \tag{13}$$

Because the bound sheet is constrained to the plate, its velocity is determined by the prescribed motion of the body. This introduces a kinematic boundary condition,

$$\mathrm{Re}\left[\hat{n}(t) \frac{\partial \overline{z}}{\partial t}(\alpha, t) \right] = \mathrm{Re}\left[\frac{\hat{n}(t)}{2\pi i} \left(\mathrm{PV} \int_{-1}^{1} \frac{\gamma(\alpha', t)}{z(\alpha, t) - z(\alpha', t)} \frac{\partial s}{\partial \alpha'}(t) \, \mathrm{d}\alpha' + \int_0^{\Gamma^-(t)} \frac{\mathrm{d}\Gamma'}{z(\alpha, t) - z(\Gamma', t)} \right) \right] \tag{14}$$

where the operation $\mathrm{Re}(\mathbf{a}\overline{\mathbf{b}}) = \mathbf{a}\cdot\mathbf{b}$ is a dot product when $\mathbf{a},\mathbf{b}\in\mathbb{C}$ are viewed as vectors in $\mathbb{R}^2$. In other words, the kinematic boundary condition states that the fluid does not penetrate the plate [4]. An additional constraint is imposed at the trailing edge. The vortex sheet strength $\gamma(\alpha,t)$ takes on the general form

$$\gamma(\alpha,t) = \frac{\sigma(\alpha,t)}{\sqrt{1-\alpha^2}} \tag{15}$$

with inverse square root singularities at the leading and trailing edge. $\sigma(\alpha,t)$ is known as the plate suction, and it is the bounded part of $\gamma(\alpha,t)$ [11]. We enforce a version of the Kutta condition that $\gamma(-1,t)$ is finite. As a consequence, this gives the following condition on the plate suction at the trailing edge:

$$\sigma(-1,t) = 0 \tag{16}$$

A final constraint comes from the conservation of circulation. Because the plate is started from rest in quiescent background fluid, Kelvin's circulation theorem gives that the total circulation must remain 0 at all time [2]. In particular, the circulation in the free and bound vortex sheets must sum to 0, with the following form given in [11] for an extensible sheet:

$$\int_{-1}^{1}\gamma(\alpha,t)\frac{\partial s}{\partial\alpha}(t)\mathrm{d}\alpha + \Gamma^{-}(t) = 0 \tag{17}$$

We are unable to enforce the Kutta condition at the leading edge without either over-constraining the system or shedding a vortex sheet from the leading edge. As a result, we limit our investigation to small-amplitude motions, corresponding physically to attached flow with minimal separation before the trailing edge, and corresponding numerically to small values of $\sigma(1,t)$.

For a flat plate, the pressure jump $[p](\alpha,t)$ across the bound sheet is given in material coordinates as the differential equation

$$\frac{\partial[p]}{\partial\alpha}(\alpha,t) = \frac{\partial s}{\partial\alpha}(t)\frac{\partial\gamma}{\partial t}(\alpha,t) + \left(\mu(\alpha,t)-\tau(\alpha,t)\right)\frac{\partial\gamma}{\partial\alpha}(\alpha,t) + \gamma(\alpha,t)\frac{\partial\mu}{\partial\alpha}(\alpha,t) \tag{18}$$

where $\mu(\alpha,t)$ is the tangential component of fluid velocity at the plate,

$$\mu(\alpha,t) = \mathrm{Re}\left[\frac{\hat{s}(t)}{2\pi i}\left(\mathrm{PV}\int_{-1}^{1}\frac{\gamma(\alpha',t)}{z(\alpha,t)-z(\alpha',t)}\frac{\partial s}{\partial\alpha'}(t)\,\mathrm{d}\alpha' + \int_{0}^{\Gamma^{-}(t)}\frac{\mathrm{d}\Gamma'}{z(\alpha,t)-z(\Gamma',t)}\right)\right] \tag{19}$$

and $\tau(\alpha,t)$ is the tangent component of the plate velocity,

$$\tau(\alpha,t) = \mathrm{Re}\left[\hat{s}(t)\frac{\partial\overline{z}}{\partial t}(\alpha,t)\right] \tag{20}$$

where $\hat{s}(t)$ is the unit tangent vector [11]. There are two components to the reaction force: a normal component due to the pressure jump across the sheet, and a tangential component of suction force as a result of the singularity in sheet strength at the leading edge. Away from the leading edge, a differential force over a material length $\mathrm{d}\alpha$ is given exclusively by the pressure acting normal to the sheet, with a differential relationship $\mathrm{d}F(\alpha,t) = -[p](\alpha,t)\hat{n}(t)\partial_\alpha s(t)\,\mathrm{d}\alpha$ [5]. The suction force at the leading edge is given by $(\pi/8)\sigma(1,t)^2$, depending only on the suction parameter at the leading edge [5]. The combination of these forces gives the net force acting on the body,

$$F(t) = \frac{\pi}{8}\sigma(1,t)^2\hat{s}(t) - \int_{-1}^{1}[p](\alpha,t)\hat{n}(t)\frac{\partial s}{\partial\alpha}(t)\,\mathrm{d}\alpha \tag{21}$$

Fang et al. [5] gives the integral expression for the input power, P_{in},

$$P_{\mathrm{in}}(t) = \int_{-1}^{1}[p](\alpha,t)\,\mathrm{Re}\left[\hat{n}(t)\frac{\partial\overline{z}}{\partial t}(\alpha,t)\right]\frac{\partial s}{\partial\alpha}(t)\,\mathrm{d}\alpha \tag{22}$$

Finally, the Froude efficiency can be computed by

$$\eta = \frac{U\langle F_x\rangle}{\langle P_{\mathrm{in}}\rangle} \tag{23}$$

where $\langle\cdot\rangle$ denotes the time-average, taken after the system reaches a periodic steady state, and F_x is the horizontal component of force, i.e. the thrust.

2.3 Desingularized Model

The purpose of this section is to modify the above equations in a manner convenient for discretization. The first concern is that the Birkhoff-Rott equation is physically ill-posed, with the free vortex sheet developing an infinite curvature singularity in finite time. The work of Krasny [7] seeks to desingularize the Birkhoff-Rott equation by introducing a small smoothing parameter, $\delta > 0$, and defining the regularized Birkhoff-Rott kernel for fixed δ,

$$K_\delta(z) := \frac{|z|^2}{|z|^2+\delta^2} \cdot \frac{1}{z} = \frac{\overline{z}}{|z|^2+\delta^2} \tag{24}$$

We notice that $K_\delta(z)$ is nonsingular for all $\delta > 0$, which allows us to modify the principal value integral in (12) as follows:

$$\mathrm{PV}\int_0^{\Gamma^-(t)} \frac{\mathrm{d}\Gamma'}{z(\Gamma,t)-z(\Gamma',t)} \approx \int_0^{\Gamma^-(t)} K_\delta\big(z(\Gamma,t)-z(\Gamma',t)\big)\mathrm{d}\Gamma' \tag{25}$$

We will make additional use of a substitution $\alpha = -\cos\phi$, with corresponding differential relationship $\mathrm{d}\alpha = \sin\phi\,\mathrm{d}\phi$. With this substitution, the vortex sheet strength can be equivalently written as

$$\gamma(-\cos\phi,t) = \frac{\sigma(-\cos\phi,t)}{\sin\phi} \tag{26}$$

We also note that $\partial_\alpha s(t) = L(t)$ with the parameterization given in Section 2.1. Taking these facts together with the δ-regularized kernel allows (13) to be written as

$$\frac{\partial\overline{z}}{\partial t}(\Gamma,t) = \frac{1}{2\pi i}\left(\int_0^\pi \frac{\sigma(-\cos\phi,t)}{z(\Gamma,t)-z(-\cos\phi,t)}L(t)\,\mathrm{d}\phi + \int_0^{\Gamma^-(t)} K_\delta\big(z(\Gamma,t)-z(\Gamma',t)\big)\,\mathrm{d}\Gamma'\right) \tag{27}$$

Similarly, the kinematic boundary condition given as (14) can be written as

$$\begin{aligned}\mathrm{Re}\left[\hat{n}(t)\frac{\partial\overline{z}}{\partial t}(-\cos\phi,t)\right] = \mathrm{Re}\Bigg[\frac{\hat{n}(t)}{2\pi i}\Bigg(&\mathrm{PV}\int_0^\pi \frac{\sigma(-\cos\phi',t)}{z(-\cos\phi,t)-z(-\cos\phi',t)}L(t)\,\mathrm{d}\phi' \\ &+ \int_0^{\Gamma^-(t)} \frac{\mathrm{d}\Gamma'}{z(-\cos\phi,t)-z(\Gamma',t)}\Bigg)\Bigg]\end{aligned} \tag{28}$$

We retain the constraint equation (16), and we rewrite Kelvin's circulation theorem from (17) as:

$$\int_0^\pi \sigma(-\cos\phi,t)L(t)\,\mathrm{d}\phi + \Gamma^-(t) = 0 \tag{29}$$

We are also able to write the pressure jump across the sheet in the concise form

$$[p](\alpha,t) = \int_{-1}^{\alpha}\frac{\partial}{\partial t}\Big(L(t)\gamma(\alpha',t)\Big)\,\mathrm{d}\alpha' + \big(\mu(\alpha,t)-\tau(\alpha,t)\big)\gamma(\alpha,t) + \frac{\mathrm{d}\Gamma^-}{\mathrm{d}t}(t) \tag{30}$$

where the integral is given by

$$\int_{-1}^{\alpha}\frac{\partial}{\partial t}\Big(L(t)\gamma(\alpha',t)\Big)\,\mathrm{d}\alpha' = \frac{\mathrm{d}L}{\mathrm{dt}}(t)\int_0^\phi \sigma(-\cos\phi',t)\,\mathrm{d}\phi' + L(t)\int_0^\phi \frac{\partial\sigma}{\partial t}(-\cos\phi',t)\,\mathrm{d}\phi' \tag{31}$$

The details of the derivation are provided in Appendix A. The force may then be computed as

$$F(t) = \frac{\pi}{8}\sigma(1,t)^2\hat{s}(t) - \int_0^\pi [p](-\cos\phi,t)\hat{n}(t)L(t)\sin\phi\,\mathrm{d}\phi \tag{32}$$

and the power may be computed as

$$P_{\mathrm{in}}(t) = \int_0^\pi [p](-\cos\phi,t)\,\mathrm{Re}\left[\hat{n}(t)\frac{\partial\overline{z}}{\partial t}(-\cos\phi,t)\right]L(t)\sin\phi\,\mathrm{d}\phi \tag{33}$$

2.4 Numerical Method

The purpose of this section is to describe the numerical method utilized to compute the vortex sheet motion. The equations introduced in 2.3, when discretized, constitute the entirety of the numerical method. We solve these equations at $N_t + 1$ discrete times $t_i = i\Delta t$, where $i \in \{0, \dots, N_t\}$ and Δt is a fixed timestep. We first discretize the body into $N_b + 1$ Chebyshev nodes at material coordinates $\alpha_k = -\cos\phi_k$ and N_b collocation nodes at material coordinates $\alpha_l^c = -\cos\psi_l$, where ϕ_k and ψ_l are given respectively by

$$\phi_k = \frac{k\pi}{N_b}, \qquad k = 0, \dots, N_b \tag{34}$$

$$\psi_l = \frac{(2l+1)\pi}{2N_b}, \qquad l = 0, \dots, N_b - 1 \tag{35}$$

We evaluate and store the values $z_k(t) := z(s(\alpha_k, t), t)$ and $z_l^c(t) := z(s(\alpha_l^c, t), t)$ at each time t_i and each sampled material coordinate, as well as the corresponding time derivatives. The analytical expression for the body position is given in Section 2.1.

At each timestep, we append a discrete point to the free vortex sheet a small distance away from the trailing edge. We initialize the free sheet at time $t = t_0$ by placing an initial point $\zeta_0(t_0)$ marked by circulation $\Gamma_0 = 0$. At each subsequent time t_i, we perform the following steps:

1. Compute the quantities $\sigma_k := \sigma(\alpha_k, t_i)$ and $\Gamma_i := \Gamma^-(t_i)$ by evaluating (16), (28), and (29).
2. Append a point $\zeta_i(t_i)$ marked by circulation Γ_i some small distance ϵ away from the trailing edge.
3. Approximate and store the free sheet velocity for each point $\zeta_j(t_i)$ on the free sheet by evaluating (27). Since we append one point at each timestep, this corresponds to $j \in \{0, \dots, i\}$.
4. Approximate the new free sheet positions $\zeta_j(t_{i+1})$ by integrating the free sheet velocity in time, where $j \in \{0, \dots, i\}$.

With the data from each timestep, we can compute the pressure jump distribution $[p](\alpha_k, t_i)$ along the sheet, followed by the net force $F(t_i)$ and the input power $P_{\text{in}}(t_i)$.

The following sections will describe the discretizations and numerical considerations in greater detail. For notational convenience, we drop notation of time dependence in these sections, noting that all quantities are evaluated at the same discrete time unless otherwise noted. We also choose to notate the number of points discretizing the free sheet as N_f, which is equal in our method to the number of timesteps which have elapsed.

2.4.1 Bound Sheet

This section details the simultaneous solution of the constraint equations (16), (28), and (29). We seek values for $\sigma_0, \dots, \sigma_{N_b}$ at the Chebyshev nodes, as well as the free sheet circulation Γ^-. We first note that the Kutta condition can be discretized immediately, with (16) becoming:

$$\sigma_0 = 0 \tag{36}$$

Next, we enforce the kinematic boundary condition given in (28) along each segment of the body. To do so, we evaluate the non-regularized integral directly at the collocation nodes, integrating over the Chebyshev nodes. We discretize the integrals using the trapezoid rule, which gives the following expression:

$$\operatorname{Re}\left[\hat{n}\frac{\partial \overline{z}_l^c}{\partial t}\right] = \operatorname{Re}\left[\frac{\hat{n}}{2\pi i}\left(L\sum_{k=0}^{N_b}\frac{w_k\sigma_k}{z_l^c - z_k} + \sum_{j=0}^{N_f-1}\frac{\Gamma_{j+1}-\Gamma_j}{2}\left(\frac{1}{z_l^c - \zeta_{j+1}} + \frac{1}{z_l^c - \zeta_j}\right)\right)\right] \tag{37}$$

where w_k is given by

$$w_k = \begin{cases} \frac{\pi}{2N_b}, & k \in \{0, N_b\} \\ \frac{\pi}{N_b}, & k \in \{1, \dots, N_b - 1\} \end{cases} \tag{38}$$

The kinematic boundary condition holds for every $l \in \{0, \dots, N_b - 1\}$. We note that $\Gamma_{N_f} = \Gamma^-$ is unknown, coinciding with vortex sheet position $\zeta_{N_f} = z_0$, the location of the trailing edge. We can rearrange (37) to isolate all known

quantities to the left-hand side, resulting in the following expression:

$$\begin{aligned}\mathrm{Re}\left[\hat{n}\left(\frac{\partial\overline{z}_l^c}{\partial t}-\frac{1}{2\pi i}\left(\sum_{j=0}^{N_f-2}\frac{\Gamma_{j+1}-\Gamma_j}{2}\left(\frac{1}{z_l^c-\zeta_{j+1}}+\frac{1}{z_l^c-\zeta_j}\right)-\frac{\Gamma_{N_f-1}}{2}\left(\frac{1}{z_l^c-z_0}+\frac{1}{z_l^c-\zeta_{N_f-1}}\right)\right)\right)\right] \\ =\mathrm{Re}\left[\frac{\hat{n}}{2\pi i}\left(L\sum_{k=0}^{N_b}\frac{w_k\sigma_k}{z_l^c-z_k}+\frac{\Gamma^-}{2}\left(\frac{1}{z_l^c-z_0}+\frac{1}{z_l^c-\zeta_{N_f-1}}\right)\right)\right]\end{aligned} \tag{39}$$

Finally, we can discretize Kelvin's circulation theorem given in (29) as follows:

$$L\sum_{k=0}^{N_b}w_k\sigma_k+\Gamma^-=0 \tag{40}$$

Altogether, Equation (39), (36) and (40) provide N_b+2 linear equations in N_b+2 unknowns $\sigma_0,\ldots,\sigma_{N_b},\Gamma^-$, which allows all quantities to be found with a linear solver.

2.4.2 Free Sheet

At each timestep, we append a point ζ_{N_f} to the free sheet, with an associated circulation Γ^-. While we solve the system of equations in 2.4.1 assuming that ζ_{N_f} is placed exactly on the trailing edge, we must actually assign the initial location some small distance away to avoid singularities. We place ζ_{N_f} a small distance away in the tangential direction,

$$\zeta_{N_f}=z_0-\epsilon\hat{s} \tag{41}$$

where ϵ is a small parameter. With moderate amplitudes of L_0, we observe that the rapid lengthening of the body can cause the body to split apart the free sheet in an unpredictable and non-physical manner, causing numerical instability which significantly affects both the free sheet dynamics and the accuracy of force and power computations. An example of this phenomenon is shown in Figure 1.

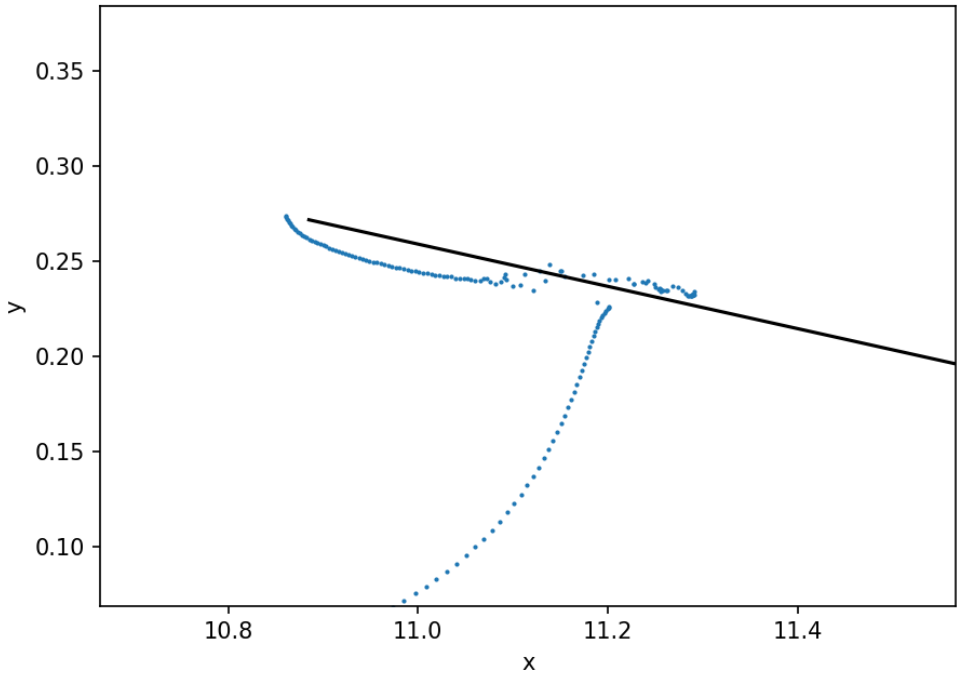


Figure 1. Example of numerical instability in the free sheet with small-amplitude heaving and pitching and a moderate lengthening amplitude $L_0 = 0.65$. Note that the free-sheet (blue) has been "sliced" by the body (black) during the extension, with the wake split between both sides of the body. A variable-ϵ approach reduces numerical noise in force and power plots up to moderate L_0, but the wake dynamics are still affected.

This phenomenon can be improved up to moderate lengthening amplitudes by choosing ϵ sufficiently large that the body does not immediately collide with ζ_{N_f} at following timesteps. However, our model assumes that the free and bound sheet form one continuous vortex sheet, which means that large values of ϵ are non-physical. Therefore, it is desirable to keep ϵ small so long as it does not cause instability. To balance these considerations, we assign ϵ according to the following rule:

$$\epsilon(t_i) = \max\left(\epsilon_0,\ -k\,\mathrm{Re}\left[\overline{\big(z_0(t_{i+1}) - z_0(t_i)\big)}\hat{s}(t_{i+1})\right]\right) \tag{42}$$

where $0 < \epsilon_0 \ll 1$ is a small, fixed parameter, $\mathrm{Re}\left[\overline{(z_0(t_{i+1}) - z_0(t_i))}\hat{s}(t_{i+1})\right]$ is the extension which the plate will see at the following timestep in the direction opposite the motion of the plate, and k is a constant weight which multiplies the extension. Note that shedding occurs a moderate distance away from the trailing edge only near the peak extension, where the trailing edge may experience a relative leftward velocity.

We can approximate the free sheet velocity by evaluating a discretized version of (27). When discretized by the trapezoid rule, we obtain:

$$\frac{\partial\overline{\zeta}_j}{\partial t} = \frac{1}{2\pi i}\left[L\sum_{k=0}^{N_b}\frac{w_k\sigma_k}{\zeta_j - z_k} + \sum_{k=0}^{N_f-1}\frac{\Gamma_{k+1}-\Gamma_k}{2}\left(K_\delta(\zeta_j-\zeta_{k+1}) + K_\delta(\zeta_j-\zeta_k)\right)\right] \tag{43}$$

where $j \in \{0,\dots,N_f\}$ indexes the points on the free sheet, and z_k are the points on the body sampled at the Chebyshev nodes. To advance the free sheet, we integrate in time using the two-step Adams-Bashforth method. For the newest point ζ_{N_f} on the free sheet, we instead utilize Euler's method because there is no previous velocity data at this point.

2.4.3 Performance Metrics

Assuming relevant data is stored at discrete times t_i, it is now possible to compute the pressure distribution across the plate, which is required to compute the net force and power input on the body. We first determine the pressure jump at the Chebyshev nodes. We note that the quantity $\tau(-\cos\phi_k, t_i)$ can be determined directly, the circulation shedding rate $\mathrm{d}\Gamma^-/\mathrm{d}t$ can be approximated by second-order backward difference, and the sheet strength, given by $\gamma(-\cos\phi_k, t_i) = \sigma_k/\sin\phi_k$, is known from simulation data. The integral term given in (31) can be approximated by the trapezoid rule, where $\partial_t\sigma_k$ may also be approximated by second-order backward difference. This leaves the tangential fluid velocity $\mu(-\cos\phi_k, t_i)$, which cannot be immediately computed at the Chebyshev nodes. We instead compute μ at the collocation nodes, using a discrete cosine transform to interpolate the values at the Chebyshev nodes. This provides sufficient information to compute the pressure.

With the pressure known, we can compute the force and input power by discretizing 32 and 33 respectively with the trapezoid rule. From here, we take a time average over the periodic steady state to obtain the time-averaged force and input power. As a consequence of the increasing sheet size, our vortex sheet method experiences quadratic slowdown as the number of timesteps is increased. To maintain reasonable computational time, we take the time average starting from an initial time after two periods of the body motion have elapsed, and ending after four total periods of the body motion have elapsed. The time-averaged force and input power are then used to compute the Froude efficiency, η.

2.5 Optimization Method

The purpose of this section is to outline the procedure for identifying optimally efficient parameters. We choose to optimize over the parameter set

$$\mathbf{x} = \begin{bmatrix} h_0 & \theta_0 & \phi_\theta & L_0 & \phi_L \end{bmatrix}^\top \tag{44}$$

Instead of optimizing over frequency directly, we choose to fix frequencies of interest and repeat the optimization, where we will consider the cases $f_L = f$ and $f_L = 2f$ separately while holding $\alpha_0 = 1$ fixed in all trials. We also fix simulation parameters $\delta = 0.2$ and $\Delta t = 0.005$ for all trials. We define our objective function in terms of the Froude efficiency,

$$g(\mathbf{x}) := -\eta(\mathbf{x}, U, f) \tag{45}$$

where the sign convention allows us to formulate the optimization as a minimization problem. We utilize the quasi-Newton method provided by the limited-memory Broyden-Fletcher-Goldfarb-Shanno algorithm with bounds (L-BFGS-B). We utilize this method so that we can set constraints on the parameter space, which is necessary for

two reasons. First, this prevents the optimizer from exploring large-amplitude motions, where the results may no longer be accurate with the model assumptions. The more important reason, however, is to prevent amplitudes from switching signs during the optimization process, which is equivalent to a discontinuous jump in phase angle. We choose the following set of constraints:

$$\begin{aligned} h_0 &\in [0, 1] \\ \theta_0 &\in [0, \pi/4] \\ \phi_\theta &\in [0, 2\pi] \\ L_0 &\in [0, 1] \\ \phi_L &\in [0, 2\pi] \end{aligned} \tag{46}$$

We note that optimal results obtained with L-BFGS-B are only expected to be locally optimal, corresponding to a local minimum of the objective function subject to the above constraints.

To compute numerical derivatives, we utilize a complex step method, which provides better accuracy than finite difference methods with similar computational cost [10]. To calculate complex derivatives, we implement the algorithm described in Section 2.4 in terms of equivalent real-valued vector operations and apply a complex perturbation in the input parameters.

3 Preliminary Results

This section details the findings of our preliminary investigation. We optimize at fixed reduced frequencies $f^* = 0.2$, 0.4, and 0.6, and report the parameter set which produces an optimal value of the Froude efficiency. We report all angles in degrees, and we non-dimensionalize h_0 and L_0 with respect to the mean chord length c. In all results, we keep three significant figures. Table 1 shows the locally optimal parameters found with L-BFGS-B and their associated Froude efficiencies when lengthening occurs twice per period, while Table 2 shows locally optimal parameters with lengthening occurring once per period.

Table 1. Parameters locally optimizing Froude efficiency with lengthening occurring twice per period. All data was obtained with an initial guess $\mathbf{x}_0 = \begin{bmatrix} 0.5 & 15^\circ & 225^\circ & 0.6 & 65^\circ \end{bmatrix}^\top$. Note that motions with large leading edge suction may attain Froude efficiencies in excess of 1.

f^*	0.2	0.4	0.6
h_0/c	3.29×10^{-5}	4.94×10^{-8}	1.62×10^{-2}
θ_0	0.00°	1.76°	6.50°
ϕ_θ	–	243°	258°
L_0/c	0.00	0.434	0.304
ϕ_L	–	59.7°	49.9°
η	0.614	2.42	1.74
$\langle \lvert\sigma(1,t)\rvert \rangle$	6.70×10^{-5}	5.52×10^{-2}	0.351

Table 2. Parameters locally optimizing Froude efficiency with lengthening occurring once per period, with maximum length achieved on the upstroke. All data was obtained with an initial guess $\mathbf{x}_0 = \begin{bmatrix} 0.5 & 15^\circ & 225^\circ & 0.6 & 65^\circ \end{bmatrix}^\top$. Note that motions with large leading edge suction may attain Froude efficiencies in excess of 1.

f^*	0.2	0.4	0.6
h_0/c	1.22×10^{-5}	0.00	1.42×10^{-8}
θ_0	0.00°	3.93°	1.37°
ϕ_θ	–	253°	256°
L_0/c	0.500	0.483	0.327
ϕ_L	32.8°	77.2°	72.5°
η	0.770	1.26	1.42
$\langle \lvert\sigma(1,t)\rvert \rangle$	2.62×10^{-5}	0.174	7.42×10^{-2}

We stress that the results presented in this section are preliminary, as there are substantial limitations in our method which require further investigation. Specific limitations and directions for future work are discussed in Section 4.

3.1 Dynamics of Lengthening-Based Maneuvers

To better understand the effects of our lengthening scheme, we present images of the wake dynamics corresponding to a parameter set $\mathbf{x} = \begin{bmatrix} 0.05 & 15^\circ & 225^\circ & L_0 & 65^\circ \end{bmatrix}^\top$, where we consider $L_0 = 0$ and $L_0 = 0.5$ with once- and twice-periodic extension. In all cases, we look at a reduced frequency $f^* = 0.4$ with images generated after four periods of motion.

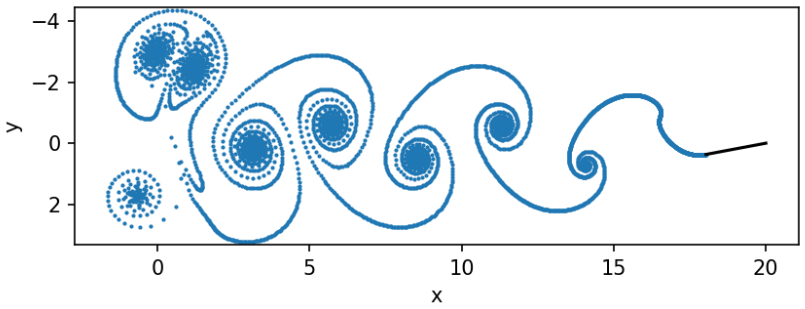


Figure 2. Wake dynamics with $L_0 = 0$. The wake can be recognized as a reverse Kármán vortex street [2]. The efficiency of this motion is $\eta = 0.399$.

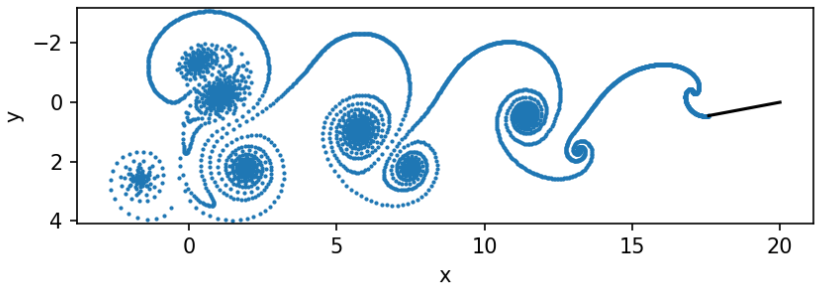


Figure 3. Wake dynamics with $L_0 = 0.5$ and extension once per period. Note that the reverse Kármán vortex street is asymmetrically distorted due to the extension of the plate. The efficiency of this motion is $\eta = 0.435$.

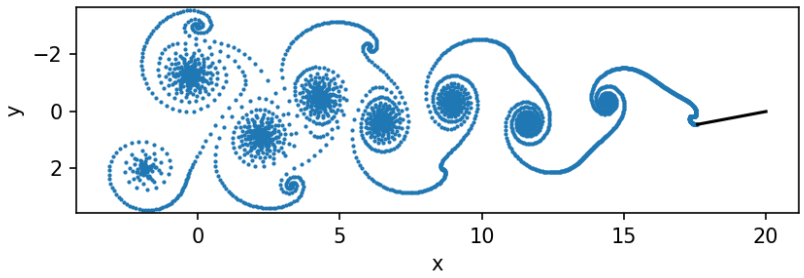


Figure 4. Wake dynamics with $L_0 = 0.5$ and extension twice per period. Note that the wake is again symmetric. The efficiency of this motion is $\eta = 0.263$.

In the above examples, the dynamics of the wake are substantially affected by the lengthening motion of the plate. The extension and retraction of the plate has a tendency to disrupt the reverse Kármán vortex street which is recognizable in the wake behind a rigid plate, shown in Figure 2.

4 Discussion and Future Work

The purpose of this section is to highlight the importance of certain results and address certain limitations which necessitate further investigation.

We first note that the Froude efficiency is very large for some motions. An explanation for this phenomenon is that moderate or large values of $\sigma(1,t)$ can induce a suction force which is much larger than the pressure drag experienced by the body, resulting in a large net thrust force. As discussed in Section 2.2, the leading edge suction should ideally be zero, but to avoid over-constraining our model, we are forced to compromise and keep the leading edge suction small. In several motions identified by the L-BFGS-B optimizer, the leading edge suction is moderate or large, resulting in large thrust relative to input power and therefore artificially large efficiency. A possible direction in future work would be to optimize subject to a penalty on $\langle|\sigma(1,t)|\rangle$, with an understanding that an optimal Froude efficiency is no longer guaranteed with this approach [10].

We have also identified several issues which prevent convergence in L-BFGS-B under certain conditions. First, optimization with frequency as a varied parameter tends to produce low-frequency "gliding" motions, similar to the results for $f^* = 0.2$ in Table 1 and 2. These motions are characterized by near-zero thrust and near-zero input power, and it is possible that the efficiency is singular as f^* approaches zero, which would represent a limitation of the model. A possible solution may involve improving the model by accounting for skin friction at a target Reynolds number, as is done in Alben et al. [1].

Another issue arises beginning at moderate values of L_0, at which point the free sheet has a tendency to "tangle" with the body, causing numerical instability. Even with the variable-distance shedding approach detailed in 2.4.2, there is no guarantee of stability, and tangling is still observed for certain motions. Tangling can induce singular velocities as points on the free sheet pass near points discretizing the bound sheet, the result of which is noisy gradients and possible divergence during the line search step of L-BFGS-B [10]. It may be necessary to introduce a "fencing" procedure, similar to that utilized by Loo and Alben [9], in order to stabilize the interaction between the free sheet and the body.

With qualifications regarding the validity of our results noted, we highlight interesting qualitative features of efficient motions. In all cases, we observe that small pitching and heaving amplitudes are favorable at low frequency, with a general benefit from larger pitching and heaving at greater frequency. We observe that at $f^* = 0.4$ and $f^* = 0.6$, similar optimal lengthening amplitudes are observed in the cases of lengthening once and twice per period, although twice-periodic lengthening is more efficient. This trend does not hold for small frequencies, where the energetic cost of lengthening twice per period outweighs additional thrust generation but is maximally beneficial when lengthening once per period.

Finally, we conjecture that motions similarly efficient to those presented in Table 2 could be obtained if maximum extension is achieved on the downstroke instead of the upstroke. Future work should confirm this by performing optimizations with variations in the initial parameter set, which may reveal the existence of different efficient classes of motion.

5 Conclusion

In this work, we investigate the aerodynamic performance of thin plates undergoing periodic maneuvers involving combined pitching, heaving, and chordwise extension. We employ a vortex sheet method to model the fluid-body interaction, including the wake dynamics and net forces on the body. We utilize the quasi-Newton method L-BFGS-B to optimize over a moderate set of parameters at fixed reduced frequencies, obtaining local maxima of the Froude efficiency. Qualitative distinction is observed between optimal motions at different frequencies, but future work is necessary to determine how numerical instabilities associated with lengthening affect the present results.

6 Acknowledgments

I would like to sincerely thank Dr. Silas Alben and Pranav Jois for their mentorship throughout this project. This work would not have been possible without their constant support, for which I am very grateful.

References

[1] Silas Alben et al. "Dynamics of freely swimming flexible foils". In: *Physics of Fluids* 24 (2012).
[2] George Batchelor. *An Introduction to Fluid Dynamics*. 1st ed. Cambridge University Press, 1967.
[3] Longfei Cong et al. "Aerodynamic performance of low aspect-ratio flapping wing with active wing-chord adjustment". In: *Journal of Fluids and Structures* 122 (2023).
[4] Jeff Eldredge. *Mathematical Modeling of Unsteady Inviscid Flows*. 1st ed. Springer Publishing Company, 2019.
[5] Fang Fang et al. "A computational model of the flight dynamics and aerodynamics of a jellyfish-like flying machine". In: *Journal of Fluid Mechanics* 819 (2017), pp. 621–655.
[6] Marvin Jones. "The separated flow of an inviscid fluid around a moving flat plate". In: *Journal of Fluid Mechanics* 167 (2003), pp. 405–441.
[7] Robert Krasny. "A study of singularity formation in a vortex sheet by the point-vortex approximation". In: *Journal of Fluid Mechanics* 167 (1986), pp. 65–93.
[8] Kang Liu et al. "Effects of dynamical chordwise retraction and stretching on the propulsive performance of a pure plunging flat plate". In: *AIP Advances* 13 (2023), pp. 025347-1 –025347-15.
[9] Yu Jun Loo and Silas Alben. "Falling plates with leading-edge vortex shedding". In: *Physical Review Fluids* 10 (2025).
[10] Joaquim R. R. A. Martins and Andrew Ning. *Engineering Design Optimization*. 1st ed. Cambridge University Press, 2021.
[11] Christina Mavroyiakoumou and Silas Alben. "Large-amplitude membrane flutter in inviscid flow". In: *Journal of Fluid Mechanics* 891 (2020), A23-1 –A23-34.
[12] Philip Saffman. *Vortex Dynamics*. 1st ed. Cambridge University Press, 1992.
[13] Jianxiong Sheng et al. "Simulating Vortex Wakes of Flapping Plates". In: *Natural Locomotion in Fluids and on Surfaces*. Vol. 155. 2012, pp. 255–262.
[14] Stephanie C. Steele et al. "Shape of retracting foils that model morphing bodies controls shed energy and wake structure". In: *Journal of Fluid Mechanics* 805 (2016), pp. 355–383.
[15] Tyler Van Buren, Daniel Floryan, and Alexander J Smits. "Scaling and Performance of Simultaneously Heaving and Pitching Foils". In: *AIAA Journal* 57 (2018), pp. 3666–3677.

A Pressure Jump Equation

The purpose of this section is to derive the pressure jump equation for a length-changing plate. We start from the differential form in terms of material coordinates, provided by Mavroyiakoumou and Alben [11],

$$\frac{\partial [p]}{\partial \alpha} = \frac{\partial s}{\partial \alpha}\frac{\partial \gamma}{\partial t} + (\mu - \tau)\frac{\partial \gamma}{\partial \alpha} + \left(\frac{\partial \mu}{\partial \alpha} - \frac{\partial s}{\partial \alpha}\nu\kappa\right)\gamma \tag{47}$$

where κ is the body curvature, which is zero for a flat plate. By adding and subtracting $\gamma\partial_\alpha\tau$, this reduces the pressure jump equation to

$$\frac{\partial [p]}{\partial \alpha} = \frac{\partial s}{\partial \alpha}\frac{\partial \gamma}{\partial t} + (\mu - \tau)\frac{\partial \gamma}{\partial \alpha} + \left(\frac{\partial \mu}{\partial \alpha} - \frac{\partial \tau}{\partial \alpha}\right)\gamma + \frac{\partial \tau}{\partial \alpha}\gamma \tag{48}$$

Combining under differentiation results in the following form,

$$\frac{\partial [p]}{\partial \alpha} = \frac{\partial s}{\partial \alpha}\frac{\partial \gamma}{\partial t} + \frac{\partial}{\partial \alpha}\left[(\mu - \tau)\gamma\right] + \frac{\partial \tau}{\partial \alpha}\gamma \tag{49}$$

With our parameterization, we note that $\partial_\alpha\tau = \partial_t L$ and $\partial_\alpha s = L$. Substituting these values and combining under differentiation gives,

$$\frac{\partial [p]}{\partial \alpha}(\alpha, t) = \frac{\partial}{\partial t}\left[L(t)\gamma(\alpha, t)\right] + \frac{\partial}{\partial \alpha}\left[(\mu(\alpha, t) - \tau(\alpha, t))\gamma(\alpha, t)\right] \tag{50}$$

Integration from -1 to α gives the following expression,

$$[p](\alpha, t) - [p](-1, t) = \int_{-1}^{\alpha} \frac{\partial}{\partial t}\Big(L(t)\gamma(\alpha', t)\Big)\mathrm{d}\alpha' + (\mu(\alpha, t) - \tau(\alpha, t))\gamma(\alpha, t) - (\mu(-1, t) - \tau(-1, t))\gamma(-1, t) \tag{51}$$

By construction, the pressure jump across the free sheet is 0, and the continuity of the pressure jump implies that $[p](-1, t) = 0$ as well [6]. Additionally, the alternative Kutta condition given by Jones [6] provides the relationship $(\mu(-1, t) - \tau(-1, t))\gamma(-1, t) = -\mathrm{d}\Gamma^-/\mathrm{d}t$. Substituting these constraints gives the equation for the pressure jump across the bound sheet in terms of material coordinates,

$$[p](\alpha, t) = \int_{-1}^{\alpha} \frac{\partial}{\partial t}\Big(L(t)\gamma(\alpha', t)\Big)\mathrm{d}\alpha' + (\mu(\alpha, t) - \tau(\alpha, t))\gamma(\alpha, t) + \frac{\mathrm{d}\Gamma^-}{\mathrm{d}t}(t) \tag{52}$$

The integral must be approximated. Since L and $\mathrm{d}L/\mathrm{d}t$ are known, we split the integral as follows:

$$\int_{-1}^{\alpha} \frac{\partial}{\partial t}\Big(L(t)\gamma(\alpha', t)\Big)\mathrm{d}\alpha' = L'(t)\int_{-1}^{\alpha} \gamma(\alpha', t)\mathrm{d}\alpha' + L(t)\int_{-1}^{\alpha} \frac{\partial \gamma}{\partial t}(\alpha', t)\mathrm{d}\alpha' \tag{53}$$

Finally, employing the substitution $\alpha = -\cos\phi$, which also gives $\mathrm{d}\alpha = \sin\phi\ \mathrm{d}\phi$,

$$\int_{-1}^{\alpha} \frac{\partial}{\partial t}\Big(L(t)\gamma(\alpha', t)\Big)\mathrm{d}\alpha' = L'(t)\int_{0}^{\phi} \sigma(-\cos\phi', t)\mathrm{d}\phi' + L(t)\int_{0}^{\phi} \frac{\partial \sigma}{\partial t}(-\cos\phi', t)\mathrm{d}\phi' \tag{54}$$

where $L(t)$ and $\mathrm{d}L/\mathrm{d}t$ are prescribed, $\sigma(-\cos\phi, t)$ is known, $\partial_t\sigma(-\cos\phi, t)$ is approximated by 2nd order backwards difference, and all integrals are discretized by the trapezoid rule.